4. Understanding QD Laser Regimes of Operation

4.1. Analytical Approximations

4.1.1. Derivation

Understanding GS-quenching is made difficult, by the high dimensionality of the system and the many experimentally not accessible variables. When described in a non-excitonic picture, one needs to at least include four different carrier reservoirs and two electric field amplitudes. Korenev et al. [KOR13a] have analytically solved a somewhat reduced representation of this system, by assuming a common hole GS level and neglecting charge conservation. They are able to derive GS-quenching light-current characteristics by assuming that holes are less likely to enter the QD than electrons. Yet they lack an explicit modelling of the current dependence.

The model used in the scope of this work contains six carrier levels and includes microscopically motivated scattering rates, which allows the realistic modelling of current dependent carrier dynamics. However, general analytical solutions, even of the steady states, do not exist. Nonetheless, an analytical approximation shall be derived in this section, which visualizes the different explanations given in the previous section. A quantitative discussion of the order of magnitude of these effects is also possible, once some general assumptions about the device are made.

The GS occupation will now be derived as the equilibrium occupation as given by the ES occupations for vanishing stimulated emission. Assuming that the carriers in the GS are mainly dominated by relaxation from the ES, all but these terms can be neglected in the time evolution of Eq. (2.63):

$$\frac{d}{dt}\rho_b^{GS} = S_{in,b}^{rel}\rho_b^{ES}\left(1-\rho_b^{GS}\right) - S_{out,b}^{rel}\rho_b^{GS}\left(1-\rho_b^{ES}\right). \tag{4.1}$$

This assumption is valid for the scattering rates as derived for self-assembled InGaAs-QDs in [LIN13, LIN14] as used for this work, as direct capture into the GS is slower than the cascade scattering from reservoir to ES and then into the GS. However, this assumption is not obviously valid in general for other material systems. Furthermore, a different electronic structure even if fabricated from InGaAs, e.g. nanorods or asymmetric QDs, could also potentially invalidate this precondition.

Solving Eq. (4.1) for the steady state of $\frac{d}{dt}\rho_b^{GS} = 0$ yields:

$$\rho_b^{GS} = \frac{1}{1+\left(\frac{1}{\rho_b^{ES}}-1\right)\frac{S_{out,b}^{rel}}{S_{in,b}^{rel}}}, \tag{4.2}$$

The ratio of in to out scattering rates can be determined by the detailed balanced relation of Eq. (2.73):

$$\frac{S_{out,b}^{rel}}{S_{in,b}^{rel}} = e^{-\frac{\Delta E_b}{k_b T}}, \tag{4.3}$$

A. Röhm, *Dynamic Scenarios in Two-State Quantum Dot Lasers,* BestMasters,
DOI 10.1007/978-3-658-09402-7_4, © Springer Fachmedien Wiesbaden 2015

Here, ΔE_b is the energy difference between GS and ES for $b \in e, h$. Hence, the GS occupation is given by:

$$\rho_b^{GS} = \frac{1}{1 + \left(\frac{1}{\rho_b^{ES}} - 1\right) e^{-\frac{\Delta E_b}{k_b T}}}, \tag{4.4}$$

by which the system can be reduced to the excited state occupations ρ_b^{ES}. Because the stimulated emission terms of Eq. (2.73) have been neglected, Eq. (4.4) can yield GS occupations that are above the GS gain clamping, which is unphysical. These can be interpreted as GS lasing states, so that the gain clamping equation turns into a threshold conditions and the lasing condition is therefore given by:

$$\rho_e^{GS} + \rho_h^{GS} - 1 \geq \frac{\kappa}{g_{GS}}. \tag{4.5}$$

After inserting the analytical approximation of Eq. (4.4) into Eq. (4.5) and reshuffling, the lengthy equation

$$\rho_h^{ES} \geq \frac{(g_{GS} + \kappa)\left(1 - \rho_e^{ES}\right) + \rho_e^{ES} \kappa e^{\frac{\Delta E_e}{k_b T}}}{(g_{GS} + \kappa)\left(1 - \rho_e^{ES}\right) + (g_{GS} - \kappa)\, \rho_e^{ES} e^{\frac{\Delta E_e + \Delta E_h}{k_b T}} + \kappa \rho_e^{ES} \left(e^{\frac{\Delta E_e}{k_b T}} + e^{\frac{\Delta E_h}{k_b T}}\right) - \kappa e^{\frac{\Delta E_h}{k_b T}}} \tag{4.6}$$

is obtained. This Eq. (4.6) expresses the lasing condition for the GS in terms of ES occupations. It is only valid for steady states, when the GS reservoirs have equilibrated with their ES counterparts. It only depends on a few key parameters: Linear gain g_{GS}, optical decay rate κ, energy spacing between levels ΔE_b and thermal energy $k_b T$. Their influence and meaning shall be discussed in the following section. By assuming that *GS occupations can be inferred from ES occupations*, the dimensionality of the system was reduced.

Lastly, expressing the ES gain clamping in terms of ES occupations is trivial, but enables the description of both ES and GS lasing thresholds in the plane of ES occupation probabilities ρ_b^{ES}. Hence, the ES is lasing if ES occupations reach sufficient values:

$$\rho_e^{ES} + \rho_h^{ES} - 1 = \frac{\kappa}{g_{ES}}. \tag{4.7}$$

4.1.2. Parameter Dependent Lasing Thresholds

Analytical expressions for both the ES gain clamping (Eq. (4.7)) and the GS lasing threshold (Eq. (4.5)) have now been obtained. For the parameters as given in Tab. 6 they are plotted in Fig. 4.1. Here, the x-axis is the ES electron occupation probability ρ_e^{ES}, while the y-axis is ES hole occupation probability ρ_h^{ES}. Yellow marks the

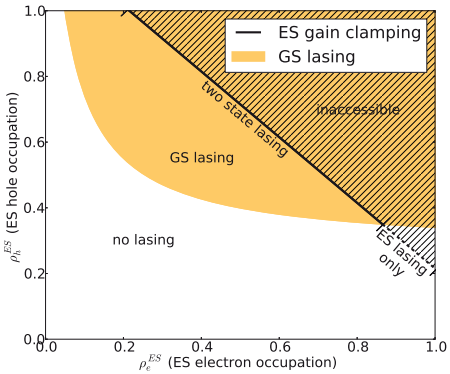

Figure 4.1: ES gain clamping and GS lasing regime vs. excited state electron and hole occupations. When the ES is lasing, the inversion is clamped at $\rho_e^{ES} + \rho_h^{ES} - 1 = \kappa/g_{ES}$ (Eq. (4.7), black line). Calculating the GS occupation probabilities through instant quasi-equilibrium yields the condition for GS lasing expressed in terms of ES occupations (Eq. (4.5), yellow area). The overlap of both corresponds to two-state lasing. Furthermore, low occupations lead to no lasing (white area). The ES occupation can never exceed ES gain clamping, hence the shaded area is inaccessible as a steady state solution. Parameters given in Tab. 6.

Table 6: Parameters used in the calculations of this section unless noted otherwise.

Symbol	Value	Meaning
T	300K	temperature
g_{GS}	0.115ps^{-1}	GS linear gain
g_{ES}	0.23ps^{-1}	ES linear gain
κ	0.05ps^{-1}	optical losses
ΔE_e	70meV	ES-GS energy gap for electrons
ΔE_h	10meV	ES-GS energy gap for holes

region where Eq. (4.5) is fulfilled and GS lasing is apparent, from here on called the 'GS lasing regime', whereas similarly the black line represents the limit of ES gain clamping (Eq. (4.5)), denoted as 'ES lasing regime'.

Thus, when reservoir densities are not relevant and the light intensity for ES and GS is only distinguished between lasing and non-lasing, the state of the system can be entirely represented by a point in ρ^{ES}-phase space. Generally, ES-occupations can lie anywhere between zero and one, but are additionally bounded by the ES gain-clamping line. The shaded area of Fig 4.1 is therefore inaccessible. The region where the GS lasing regime and the ES lasing regime intersect, i.e. where the black line lies inside the yellow area, two-state lasing is present.

However, despite this helpful visualisation of two-state lasing, current-dependent steady states are not calculable in this semi-analytical approach. They have to be calculated separately and can then be compared to the analytical approximations and boundaries in the ρ_b^{ES}-plane as later done in Sec. 4.2. But studying the extent and parameter dependence of the different lasing regimes can nevertheless yield valuable insights for the underlying mechanics of GS quenching.

Generally, Eq. (4.6) suggests that the position of the GS lasing regime and the extent of the overlap region indicating two-state lasing can be changed by changing the gain g or losses κ, the temperature T or the energy structure $\Delta E_e/\Delta E_h$. This

is reflected in some of the GS quenching mechanisms already suggested in the literature, e.g. self-heating or gain suppression by homogeneous broadening increase, but has not been discussed coherently. Therefore, a variety of parameter sets and the implications for two-state lasing shall be discussed in this section.

For the set of parameters as taken in Fig. 4.1, there is an overlap of GS and ES-lasing regimes. This 'two-state lasing regime' marks the dual-emitting state of the QD laser. Additionally, for low hole occupations, the ES gain clamping is outside the GS lasing regime bounds and solitary ES lasing is apparent. If the current dependent scattering dynamics of the laser lead to a transition from the two-state lasing regime to the solitary ES lasing regime, a quenching of the GS can be observed.

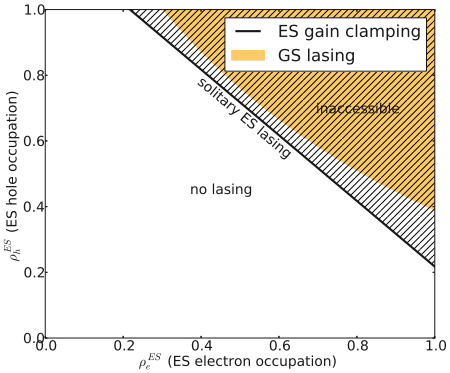

Figure 4.2: ES gain clamping and GS-lasing regime vs. ES electron and hole occupations for lower confinement ΔE_e = 15meV and ΔE_h = 5meV (other parameters given in Tab. 6). The ES gain clamping line (Eq. (4.7), black line) lies entirely outside of the GS-lasing regime (Eq. (4.5), yellow area). There is no overlap and therefore no two-state lasing regime.

The two-state lasing regime can be entirely absent for different parameters, when the GS lasing regime lies at too high ρ^{ES} to facilitate GS lasing. Figure 4.2 shows the analytical lasing regimes for lower electric confinement ΔE_e = 15meV and ΔE_h = 5meV. Here, the GS lasing regime lies entirely in the inaccessible part above the ES gain clamping line (shaded areas). This corresponds to a QD structure, where charge carriers are easily escaping the GS and both confined states have similar occupations. The ES will then be left lasing, because its higher degeneracy leads to a larger optical gain. As can be seen, two-state lasing is impossible for such a device, independent of the actual current-dependent dynamics, as the GS never turns on.

Consequently, increasing the confinement to ΔE_h = 30meV will prevent any solitary ES lasing. As seen in Fig. 4.3 the GS-lasing (yellow area) regime is covering the entire extent of the ES gain clamping line (black), which means there is no steady state of purely ES lasing. The system can and possibly will traverse the GS lasing-regime for increasing currents and end up in a two-state lasing regime on the gain clamping limit, but it has nowhere to go from there.

Note that the parameters given in Tab. 6 and the follow up examples all feature significantly smaller energetic hole confinement ΔE_h than electron confinement ΔE_e. On the one hand this is based on the microscopically calculated electronic structure of real QD devices [SCH07f], but on the other hand this has emerged in the scope of this analytical approach as a key feature of lasers exhibiting a GS-quenching

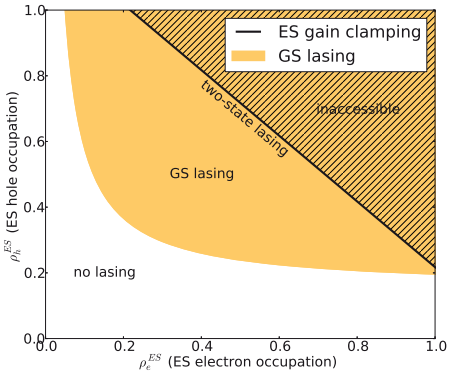

Figure 4.3: ES gain clamping and GS lasing regime vs. excited state electron and hole occupations for stronger hole confinement ΔE_h = 30meV (other parameters given in Tab. 6). No solitary ES-lasing present, as the ES gain-clamping line (black) lies entirely inside the GS-lasing regime (yellow area).

behaviour. This is in accordance with the work of Viktorov et al. [VIK05], where they proposed an asymmetry-based GS-quenching mechanism.

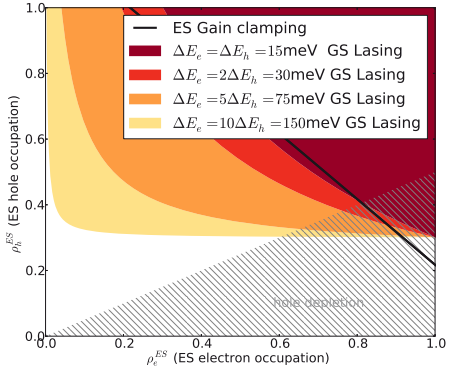

Figure 4.4: Energy asymmetry effects on GS quenching. When GS and ES energy separation is the same for holes and electrons, the ES inversion clamping (black line) is intersected symmetrically by the GS lasing regime (dark red). Because of this symmetry, electron depletion then also leads to GS quenching. This symmetry is lost for increasing electron energy separation ΔE_e. Other parameters given in Tab. 6. ©(2015) IEEE. Reprinted, with permission, from [ROE14]

The influence of this asymmetry is shown in Fig. 4.4. The electron confinement ΔE_e was changed from a symmetric case (dark red area) to an increasingly asymmetric one. While for the symmetric case low electron occupations also lead to GS quenching, only the hole depletion side retains solitary ES lasing for the asymmetric energy structures (red, orange, yellow areas).

Next, reducing the depth of the confinement for both electrons and holes in Eq. (4.6) is equivalent to increased increasing the temperatures. Figure 4.5 shows, in accordance with the phenomenological explanation of carrier escape, that high temperatures lead to a broader solitary ES lasing regime, until GS lasing becomes altogether impossible (at 1030K, dark red area). Yet, the temperature differences required to achieve a significant change in the analytical boundaries of the ρ^{ES}-phase space lie well outside of the experimentally feasible tens of Kelvins. The self-heating

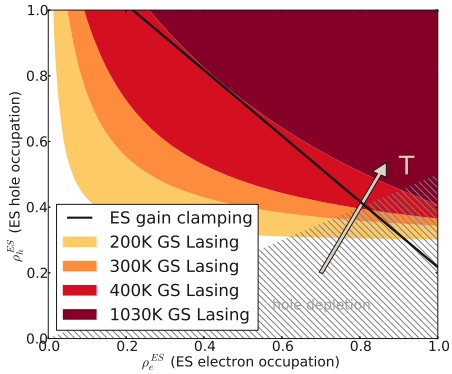

Figure 4.5: Two-state-lasing regimes as a function of excited state electron and hole occupation probabilities for different temperatures. The ES inversion clamping (black) intersects with the GS lasing regime (yellow to red) at high electron to hole ratios. With increasing temperature (darker colours) the two-state-lasing regime (overlap of ES gain clamping and GS lasing area) shrinks in size and vanishes for very high temperatures (dark red, 1030K for this set of parameters). Other parameters given in Tab. 6. ©(2015) IEEE. Reprinted, with permission, from [ROE14]

mechanism, proposed in the literature to explain GS-quenching [MAR03c, JI10], is therefore only a minor contributor in most cases. Every change in the electron-to-hole ratio has a larger impact than realistic temperature differences. Nonetheless self-heating can support the transition by widening the hole-depletion window for GS-quenching.

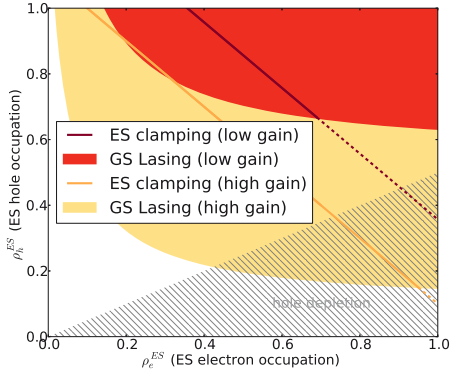

Figure 4.6: Gain dependence of GS quenching (possible on the dashed line). The low gain ($g_{GS} = 0.5g_{ES} = 0.07ps^{-1}$, red line) ES clamping is shifted to the right in comparison to the high gain scenario ($g_{GS} = 0.5g_{ES} = 0.25ps^{-1}$, orange line). The GS lasing regime is significantly larger for the high gain case (yellow area), as opposed to the low gain case (red area). Other parameters given in Tab. 6. ©(2015) IEEE. Reprinted, with permission, from [ROE14]

Lastly, the impact of the linear gain is shown in Fig. 4.6, where both the GS and ES gain were multiplied with the same factor. This is equivalent to a decrease in the optical losses κ (see Eq. (4.6)). Experimentally this corresponds to longer devices or higher QD densities. The change of size for the GS-lasing regime and solitary ES lasing regime is significant. While the low gain ($g_{GS} = 0.5g_{ES} = 0.07ps^{-1}$, red) exhibits solitary ES lasing for a wide range of ES occupations, the high gain ($g_{GS} = 0.5g_{ES} = 0.25ps^{-1}$, orange) virtually suppresses the entire GS-quenching window in the hole-depletion area. Yet despite a proposed gain decrease through homogeneous broadening [SUG05b], which has been later questioned by follow up studies [GIO12,

KOR13], the linear gain has to be treated as constant in our modelling approach. Choosing a gain of the correct magnitude is obviously of high significance, if one wants to facilitate two-state lasing, GS-quenching or solitary ES lasing. Yet, a current dependent, variable gain will not be considered from here on.

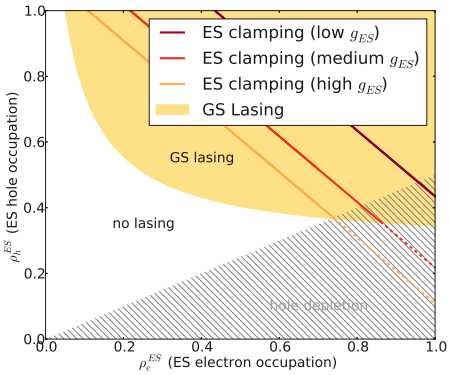

Figure 4.7: ES gain dependence of two-state lasing. When the ES gain g_{ES} is treated as an independent variable, the ES gain clamping (dark red, red, orange line) can be moved relative to the GS-lasing regime (yellow area). While the low ES gain ($g_{ES} = 0.115ps^{-1}$, dark red line) exhibits only two-state lasing, a higher ES gain ($g_{ES} = 0.23ps^{-1}$, red line and $g_{ES} = 0.46ps^{-1}$, orange line) enables solitary ES-lasing (dashed parts of the line). ©(2015) IEEE. Reprinted, with permission, from [ROE14]

When the ES gain is treated as a free parameter, instead of being always the double of the GS gain due to degeneracy, or if the ES and GS experience a different cavity, e.g. through spectral coating [ARS14], the ES gain clamping line can be easily moved relative to the GS-lasing regime. As seen in Fig. 4.7 high ES gain ($g_{ES} = 0.46ps^{-1}$, orange line) possesses a smaller two-state lasing regime and enables solitary ES lasing, whereas this is absent for low ES gain ($g_{ES} = 0.115ps^{-1}$, dark red line). The intermediate $g_{ES} = 0.23ps^{-1}$ is the reference gain assuming that $g_{ES} = 2g_{GS}$.

In summary, this semi-analytical approach allows to analyse the impact of parameter changes on the two-state lasing behaviour independent of the current-dependent occupation dynamics. Assuming realistic QD electronic structures, the window for GS-quenching is only present at low hole occupations. This is strong evidence that hole-depletion for high currents is the dominating effect leading to GS quenching. All other explanations as given in Sec. 3.3.1 play only a minor role.

The knowledge gained for choosing the right parameters will later be reflected in Sec. 4.3, where varying optical losses κ, ES gain g_{ES}, electronic confinements and temperatures T are investigated. These parametric studies are in good agreement with the analytic results that high κ, γ_{ES} and temperatures all favor solitary ES lasing, whereas strong confinement leads to a broader GS-lasing regime.

When these analytical boundaries are combined with numerically calculated, current dependent ES occupations $\rho^{ES}[J]$, the steady states of the system can be traced across the ρ^{ES}-plane. This will be done at the end of the following Sec. 4.2.

4.2. Numerical Simulation of GS Quenching

4.2.1. Modeling Approaches and Light-Current Characteristics

The numerical model introduced in Sec. 2.3 shall now be used to derive current-dependent steady states. The parameters used are the same as in Sec. 3.2 in Tab. 4. They were chosen based on previous works of Benjamin Lingnau [LIN14] and Ref. [LUE09, LUE11a, LUE12]. However, with the scattering rates as derived in Sec. 2.3.2, GS quenching is never reached. This can bee seen in the LI-curve of Fig. 3.3 on page 32.

Three different modelling approaches corresponding to the three mechanisms explained in the literature in Sec. 3.3.1 will be applied to the numerical model: Homogeneous broadening, self-heating and hole depletion. From these three the homogeneous broadening induced decrease of the gain constants g_{GS} and g_{ES} is the least physically sound. With active and inactive dots already included in the model and 'spectral holeburning' induced mechanics already approximated to a first order, any further change of gain parameters seems arbitrary.

Nevertheless, for completeness a short reproduction of the findings of Sugawara *et al.* [SUG05] shall be included. The gain of the GS and ES will be reduced with increasing overall intensity, accounting for a further broadening of the spectral line and an decreased overlap of QD ensemble and lasing wavelengths:

$$g_m = \frac{g_m^0}{1+\varphi(|E^{GS}|^2+|E^{ES}|^2)}, \tag{4.8}$$

with $m \in \{GS, ES\}$ and g_m^0 being the gain at zero intensity. The suppression coefficient φ was set to $5 \cdot 10^4[\mathrm{V/nm^2}]^{-1}$ to yield GS quenching. Fig. 4.8 shows the resulting light-current characteristic. In agreement with expectations, the GS quenching is observed. Reducing the gain is the most efficient way of suppressing lasing activity, so the inclusion of an intensity-dependent gain will naturally lower the GS gain until only ES lasing is stable. However, as neither the underlying physical process nor the magnitude of the parameters can be satisfyingly deduced from a first principle, an increase of homogeneous broadening will not be included from here on.

Self-heating was included by increasing the out-scattering rates $S_{b,out}^{m,cap}$ and $S_{b,out}^{Rel}$ according to the detailed balance condition:

$$S_{out} = S_{in} e^{-\frac{\Delta E_k}{k_b T}}, \tag{4.9}$$

where ΔE_k is the potential energy difference of the two energy levels involved in the scattering process. The temperature itself was modelled to increase linearily with pump current J, to account for the joule-heating of a device with constant voltage applied [LUE12]:

$$T = 300\mathrm{K} + DJ, \tag{4.10}$$

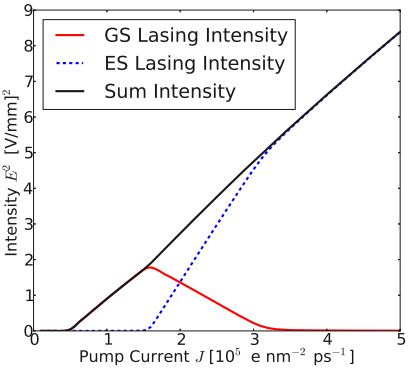

Figure 4.8: Simulated light-current characteristic for self-assembled InAs/GaAs QDs exhibiting GS quenching caused by homogeneous broadening. The GS and ES gains were modified to decrease with increasing current densities, to account for a strong increase of spectral width of lasing lines. The GS starts to decline after the onset of ES lasing, while the slope of the overall intensity stays roughly the same. Parameters as given in Tab. 4.

where the heating coefficient was chosen to be $D = 35[\mathrm{K}] \cdot 10^4[\mathrm{e/nm^2ps}]^{-1}$. The resulting GS-quenching light current characteristic is shown in Fig. 4.9. The temperature (green) rises linearly with pump current J (x-axis), while the GS intensity (red) starts to decline after the onset of ES lasing (blue). However, the temperature at which GS quenching is occurring is $T \simeq 450$K, which is higher than what most devices are able to withstand.

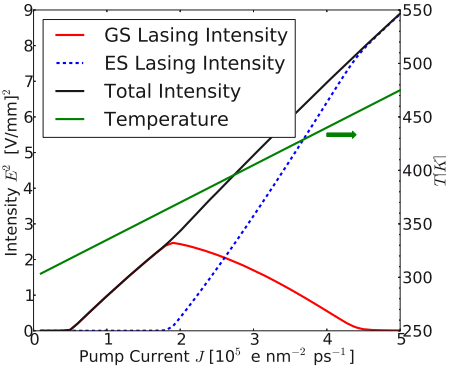

Figure 4.9: Simulated light-current characteristic for self-assembled InAs/GaAs QDs exhibiting GS quenching caused by self-heating. The temperature (green) was modelled to increase linearly with injection current J. The GS starts to decline after the onset of ES lasing, while the slope of the overall intensity stays roughly the same. Parameters as given in Tab. 4.

In favour of the self-heating hypothesis is the fact, that the carrier temperature could potentially be higher than the surrounding device temperature, as the pump current drives the system far away from thermal equilibrium. However, as already mentioned in Sec. 3.3.1, this thermal evolution should not be unique to InAs/GaAs QDs, but also be applicable to InP QDs, where GS quenching has not been observed. This leads to the conclusion that self-heating is not playing a major role in the appearance of solitary ES lasing and focuses the attention of this work on the third mechanism mentioned.

The electron-hole asymmetry leading to 'hole depletion' as first mentioned by Viktorov *et al.* [VIK05] shall now be reproduced. Subsequently, the scattering behaviour of our system was changed to achieve low hole densities by reducing the hole capture scattering rates. $S_{h,in}^{GS,cap}$ and $S_{h,in}^{ES,cap}$ were reduced to 5% of their microscopically calculated value. This is, of course, a great violation of the motivation behind calculating scattering rates microscopically and can only be justified in two ways: Either the real-world scattering rates still differ from the current microscopic model due to some processes not being accounted for, e.g. non-parabolic wavefunctions [SCH07f] or Coulomb interaction of carriers, or the energy levels used as initial preconditions for calculating the scattering dynamics are different from QDs that exhibit GS quenching. Also, Gioannini (2012) [GIO12] has shown a convincing alternative by introducing long transport times through an additional confinement structure. Including more hole states for the modelling can also help, as then by distributing the available charge carriers more evenly over the different states, the occupation of a single state is reduced.

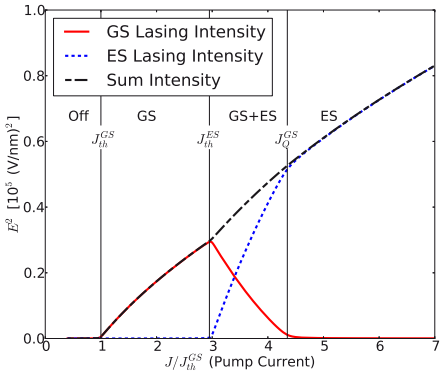

Figure 4.10: Light-current characteristic for self-assembled InAs/GaAs QDs exhibiting GS quenching caused by hole depletion. The GS intensity starts to decline after the onset of ES lasing, while the slope of the overall intensity stays roughly the same. The pump-current has been normalized to the GS lasing threshold J_{th}^{GS}. The ES lasing threshold J_{th}^{ES} and GS quenching current J_Q^{GS} are marked with vertical lines. Parameters as given in Tab. 4, with microscopically calculated scattering rates as in App. A.1 with hole capture reduced to 5%. **[Reference Parameter Set]** ©(2015) IEEE. Reprinted, with permission, from [ROE14]

Figure 4.10 shows the light-current characteristic for a hole-depletion induced GS quenching. This will serve as a reference simulation from here on to further study the hole-depletion mechanism in greater detail. As scattering rates and energy levels are highly material sensitive, the process of hole depletion is arguably the only remaining physical mechanism that sets different species of QDs apart. So, in accordance with the findings of the most recent literature [GIO12, KOR13, KOR13a], electron-hole asymmetry emerges as the major contributor for GS quenching. Therefore the rest of this chapter shall be devoted to further studying the hole-depletion induced GS-quenching mechanism.

4.2.2. Carrier Dynamics in GS Quenching

To further illustrate the driving mechanism between the transition of different lasing states, Fig. 4.11 plots the GS and ES occupations corresponding to Fig. 4.10 versus

pump current. Here only the densities of the active subensemble are shown, as they are most relevant to the lasing behavior.

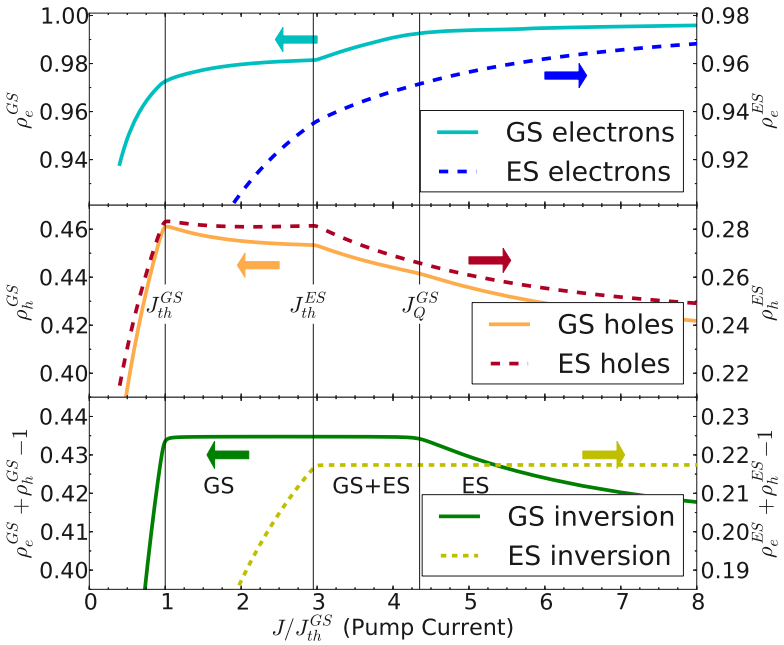

Figure 4.11: Electron (top panel) and hole (middle panel) occupation probabilities for ground (solid lines) and excited state (dashed lines) during GS quenching. Electron occupations are higher because of the higher energy spacing between QD and reservoir. Different lasing regimes are separated by vertical lines. During GS lasing the GS inversion (green solid line, bottom panel) is gain clamped until it quenches at J_Q^{GS}, the ES inversion (green dashed line, bottom) is clamped after the ES lasing threshold J_{th}^{ES}. Parameters as given in Tab. 4, with microscopically calculated scattering rates as in App. A.1 with hole capture reduced to 5%. **[Reference Parameter Set]** ©(2015) IEEE. Reprinted, with permission, from [ROE14]

Electron occupations (Fig. 4.10, top panel) are generally higher than hole occupations (Fig. 4.10, middle panel). This is caused by their higher electronic confinement of 50 meV, as opposed to only 20 meV for holes, resulting in smaller escape rates and higher equilibrium densities.

In the regime with no lasing ($J < J_{th}^{GS}$), all occupations increase with injection current J. This is caused by the overall increase of carriers and the resulting filling of states inside the reservoir, GS and ES. When GS lasing is reached at the GS threshold current $J = J_{th}^{GS}$, the GS inversion is clamped at $\rho_e^{GS} + \rho_h^{GS} = \kappa/g_{GS} + 1$ and will henceforth be constant (green solid line, bottom panel). Up until this point, the dynamics mirror a conventional laser reaching its threshold. Yet, as described

in Sec. 3.2, there is no gain clamping of the ES by the GS occupations. Naturally, when extra charge carriers are added, many of them end up getting consumed by stimulated emission and increase the the GS lasing intensity above threshold (see Fig. 4.10, red line). But due to the incomplete gain clamping, carriers will also start to fill the ES (dashed lines).

This has already been mentioned as a requirement for two-state lasing; relaxation processes must not be too fast, as otherwise the GS and ES occupations would always be close to equilibrium and the ES would also be clamped [MAR03a]. The system needs to be allowed to retain extra charge carriers in the ES, while the GS is lasing. Two-state lasing is only possible because of the ES occupations increasing despite the GS inversion being already clamped.

However, with the increased complexity introduced through the non-excitonic nature of the numerical model, an additional detail starts to emerge: It is mainly the electron occupation probability ρ_e^{ES} that is rising, whereas hole occupations do not increase inside the GS lasing regime. This can only be interpreted in one way: The GS holes are clamping the ES holes, but the ES electron occupation ρ_e^{ES} is largely independent of the corresponding GS occupation ρ_e^{GS}. The extra holes added to the system are accumulating in the well w_h and the resulting increase in the scattering $S_{h,in}^{GS,cap}$ which *should* increase hole occupations is completely overcompensated by an increased carrier recombination through stimulated emission.

The incomplete gain clamping appears to be caused by the electrons in the system, while the hole occupations are much more closely tied to each other due to the smaller energy separation $\Delta E_h < \Delta E_e$. This is also in agreement with approaches applied previously in the literature: The analytical approximations made by Viktorov *et al.* [VIK05] and Korenev *et al.* [KOR13, KOR13a], who both combined the hole GS and ES into a common level, virtually achieve the same outcome. The numerical findings of this work also resemble the instant-equilibrium approach for hole-densities applied by Gioannini (2012) [GIO12].

When ES lasing starts at the ES threshold current $J = J_{th}^{ES}$, gain clamping occurs for it as well (green dashed line in Fig. 4.11, bottom panel). This would leave an excitonic model with no further degrees of freedom for the system, but in the non-excitonic picture of this work the fraction of electrons to holes can still change. Due to the higher scattering induced input, electron densities in the ES are still rising (dashed line, top panel). ES Gain clamping will then symmetrically lower ES hole occupation (dashed line, center panel) as $\rho_h^{ES} + \rho_e^{ES} = const.$ Due to the equilibrating relaxation scattering processes, the GS is always bound to the ES and must follow the increasing electron fraction. Therefore, GS electrons are also rising while GS holes are decreasing (Fig. 4.11, middle and top panel, solid lines). This is exactly the behaviour that was assumed in the derivation of the analytical lasing boundaries of Sec. 4.1, namely that the GS occupations can be inferred from their ES counterparts.

With the increasing ES electron occupation ρ_e^{ES} rising and constantly forcing the GS electron occupation ρ_e^{GS} to follow it, ρ_e^{GS} soon reaches values above 0.99. Then, at the GS quenching threshold current ($J = J_Q^{GS}$) electron occupations in the GS are virtually filled $\left(\rho_e^{GS} \simeq 1\right)$ and can no longer increase with rising J.

Simultaneously, GS holes are still depleting to follow the ES trend. At this stage, the quasi-equilibrium occupations of the GS will fall below the inversion needed to sustain lasing and thus force the GS to quench. The quenching is aided by the high Boltzmann-factor for the electrons, which enables the ES electrons to increase even further.

For high pump currents only solitary ES lasing remains. Holes deplete even further towards higher currents, but do not alter the lasing regime. Thus, the carrier dynamics shown in Fig. 4.11 and explained in the paragraphs above nicely exemplify the underlying mechanics of the inequality given in Eq. (4.6).

To conclude, there is not only 'hole depletion' but also a 'saturation of electrons' that leads to GS quenching. The GS has to compete with the excited state for carriers, and can only do so by holes, because GS electrons are saturated.

4.2.3. Comparison with Analytical Approach

The reference simulation with light-current characteristic in Fig. 4.10 on page 46 and density dynamics shown in Fig. 4.11 will now be visualized in a third way, by combining the numerical results with the analytical approximations derived in Sec. 4.1. The analytical lasing boundaries of Eq. (4.7) and Eq. (4.6) will be displayed with the numerically calculated, current dependent ES occupations $\rho^{ES}[J]$ of the reference simulation. The steady states of the system can then be traced across the ρ^{ES}-plane and the crossing of the analytical lasing regime boundaries should correspond to a change of lasing state in the numerics.

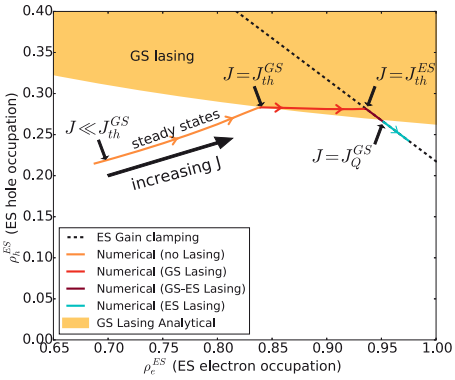

Figure 4.12: Analytically derived lasing regimes from Eq. (4.6) and numerically obtained steady state occupations ρ_e^{ES} and ρ_h^{GS} for increasing pump current J. Numerical results are colored according to the different lasing states. No lasing on the orange part of the line, red represents solitary GS lasing. When the excited state inversion is reached (black dashed line), two-state lasing happens on the dark red line and solitary ES lasing on the blue line. Parameters as in Tab. 4 on page 32, with microscopically calculated scattering rates as in App. A.1 with hole capture reduced to 5%. **[Reference Parameter Set]** ©(2015) IEEE. Reprinted, with permission, from [ROE14]

The steady states of the reference simulation in the ρ_e^{ES}-ρ_h^{ES} phase-space are shown in Fig. 4.12. Because the J-dimension is lost in this representation, the numerically derived line is color-coded according to the different lasing states.

The orange part of the line is below threshold, and as expected the numerical occupation probabilities lie outside of the analytical lasing regimes. Transition to

GS lasing (red line) is then observed as soon as the border of the GS lasing regime (yellow area) is crossed at $J = J_{th}^{GS}$. When the necessary excited state inversion is reached (black dashed line), the numerics will lead to two-state lasing (dark red line) at $J = J_{th}^{ES}$, and the system is hence forced to stay on the inversion given by the gain clamping. The fraction of electrons to holes is now the only degree of freedom left. Due to the low hole capture rates $S_{h,in}^{m,cap}$, the system approaches hole depletion and leaves the analytical GS lasing regime (yellow area) at $J = J_Q^{GS}$. This coincides with the transition to solitary ES lasing and GS quenching (cyan line) in the numerical simulation.

The agreement between analytical and numerical results in Fig. 4.12 is good, even though GS roll-over occurs for slightly lower hole occupations in the numerical model (barely visible in the plot). This can be explained by the direct capture processes from the surrounding carrier reservoir to the QD ground state, not taken into account in the analytical part. The direct capture processes slightly extend the GS lasing regime beyond the analytical approximations.

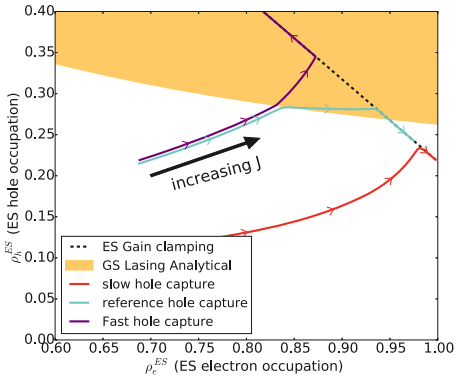

Figure 4.13: Analytical two-state lasing regime and numerical simulations of the steady states vs. excited state occupations for different hole capture scattering rates (different colours). Red are 0.5% hole capture rates, blue is our reference scattering and the pink line denotes a five times faster direct hole capture process (which is still only 25% of the microscopical scattering rates). Different regimes are crossed and lasing transitions differ accordingly. Parameters as in Tab. 4 on page 32.

The reason why hole capture rates had to be reduced to facilitate GS quenching will now be shortly highlighted, by changing the hole-capture rates and plotting the resulting J-dependant steady states in the ρ_e^{ES}-ρ_h^{ES} phase-space. As simulated in Sec. 3.2 for Fig. 3.3, with faster hole scattering rates GS quenching is absent as hole depletion is never reached. This is caused by the steady states moving to higher ρ_h^{ES} and into the stable two-state lasing regime. To illustrate this, Fig. 4.13 displays the results shown in Fig. 4.12 (cyan line) together with numerical simulations for slower (red line) and higher (pink) hole capture rates.

For the very slow hole capture process (red line), the hole occupations are suppressed so strongly that the GS lasing regime is never crossed. Consequently, the corresponding light-current characteristic then exhibits no GS lasing. This ES only lasing is similar to a high loss scenario, where light-current characteristics lack the GS transition as well. On the other hand, when hole capture rates are high (Fig. 4.13, pink line) - but still smaller than electron capture rates - the GS will never quench, as the electron-hole ratio shrinks with increasing currents. The two-state lasing state

is stable for all pump currents and GS lasing intensity will even increase after the ES switch-on.

Looking at Fig. 4.13, one might ask the question for which magnitude of hole in-scattering the hole fraction starts to reduce after the onset of two-state lasing. Somewhere between the 'fast hole capture' (pink) and 'reference hole capture' (cyan) should lie a critical scattering rate, which leads to a constant electron-to-hole fraction. The derivation of this point could then possibly lead to some mathematical condition between hole and electron scattering rates, if hole depletion is to be reached. However, this was not achieved in the time of this work and it must therefore be left for future investigations.

Overall the analytical approximation has shown itself to be very robust, owing to the large difference between relaxation scattering and GS capture scattering magnitudes. This leads to a close tying of GS occupations to their ES counterparts, while simultaneously the ES is able to avoid gain clamping by being exposed to the much larger ES capture rates.

4.2.4. Turn-On Dynamics

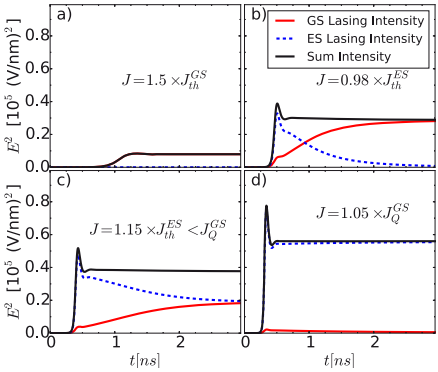

Figure 4.14: Electric field intensity turn on curves for ground and excited state lasing. Even for currents below the ES threshold (b), the ES is lasing during turn-on transient, but switches off again. During two-state lasing (c), GS is slower to converge as the ES levels fill up faster. For currents higher than the GS quenching threshold (d) GS lasing is shortly visible during relaxation oscillations. Parameters as given in Tab. 4, with microscopically calculated scattering rates as in App. A.1 with hole capture reduced to 5%. [**Reference Parameter Set**] ©(2015) IEEE. Reprinted, with permission, from [ROE14]

So far the time evolution of the electric field amplitude in the two optical modes (GS and ES) was not addressed. In this section the turn-on dynamics of the reference simulation shall be discussed for the different lasing regimes (see Fig. 4.10 for steady states). Quantum dot lasers exhibit strongly damped relaxation oscillations, as visible in Fig. 4.14 (a) for the GS turn-on inside the GS lasing regime.

However, during turn-on both optical transitions of GS and ES can be visible, even if the corresponding steady states are outside of the two-state lasing regime. As seen in Fig. 4.14 (b), ES lasing occurs temporarily for currents lower than the ES lasing threshold. Accordingly, GS lasing takes longer to increase. This is due to faster scattering into the ES levels, as well as due to the resulting slowly building up of the GS inversion clamping.

The turn-on delays of ES and GS can be analytically approximated from the effective carrier lifetime of the level and the modal gain [SOK12]. For our scattering rates and set of parameters the turn-on delay is equal for both ES and GS, so that both turn on synchronously. Note that the correlation of the relaxation oscillations, e.g. peaks coinciding in Fig. 4.14 for both lasing transitions, is caused by the fast relaxation from ES to GS. Overall, the shape and timing of the simulation is in good agreement with the experimental measurements of Ref. [DRZ10].

Inside the two-state-lasing regime at $J = 1.15J_{th}^{ES}$, the ES is again starting to lase earlier (Fig. 4.14 (c)). Ground state lasing is also visible for currents greater than the quenching threshold (Fig. 4.14 (d)). During turn-on oscillations, ES and quantum well occupations will be higher than in the eventual steady state. This allows the GS to be filled above its threshold and the transition is visible for several ns. In an experimental setup this might be useful in finding a current range that is closest to achieving two-state lasing, e.g. if ES lasing can only be started via external injection or by introducing an additional feedback loop.

Strikingly, the overall intensity (black line (a)-(d)) converges significantly faster than the individual contributions of GS and ES. Due to the time constraints of this work the exact cause of this has not been found so far. However, from a purely dynamical standpoint it is clear to say, that within the high-dimensional phase-space of laser operation the system is highly damped transversal to the plane of $|E^{GS}|^2 + |E^{ES}|^2 = const.$ But within this plane of constant overall-intensity the convergence is much slower and the real-part of the corresponding eigenvalues is supposedly closer to zero.

However, this explanation is lacking a physical mechanism explaining and quantifying the important damping factors. One might formulate the hypothesis, that charge carrier conservation forces the system to adjust its overall lasing-output to the incoming electron and hole flux on relatively short time scales. This would suggest that the damping of the overall relaxation is related to the traditional relaxation oscillation damping of single-state lasers, so that the usual calculus should be applicable. Simultaneously, the competition between modes is, arguably, linked to the difference of some 'effective gain'. Furthermore this behaviour is comparable with the turn-on dynamics of multi-mode lasers [DOK12] and is likely caused by a mechanism similar to that.

4.3. Lasing Regimes In Parameter Space

4.3.1. QD size and optical losses dependence

Inspired by the analytic results and the crucial role of the energy separations a systematic scan of the parameter space seems prudent. At first, the band structure will be continuously scaled. To do that, a linear scaling factor r is introduced. Energy spacing between levels are multiplied with r and new scattering rates are calculated for the resulting energy structure (see also App. A.2). Lower r corresponds to a more shallow energy structure, higher r for deeper QD levels (keeping the asymmetry). By looking at different steady states as a function of r, a qualitative picture for the two-state lasing behaviour of QD lasers with different sizes can be obtained.

Secondly, the optical losses κ are also varied, while keeping $g_{ES} = 2g_{GS} = 0.23ps^{-1}$ for the moment. For a better comparison with experimental findings, these optical losses can be converted into cavity lengths ℓ via the relation [LUE08]:

$$2\kappa = (2\kappa_{int} - \frac{\ln r_1 r_2}{2\ell})\frac{c}{\sqrt{\epsilon_{bg}}} \tag{4.11}$$

Where ℓ is the cavity length, r_1, r_2 are the facet reflection coefficients ($r_1 = r_2 = 0.32$ for a GaAs-air surface), c is the speed of light and $\epsilon_{bg} = 14.2$ is the background permittivity in the cavity. Internal losses of $\kappa_{int} = 110m^{-1}$ in accordance with Ref. [LUE08] were used. This formula is only valid for the Fabry-Perot type edge-emitting lasers used in this work.

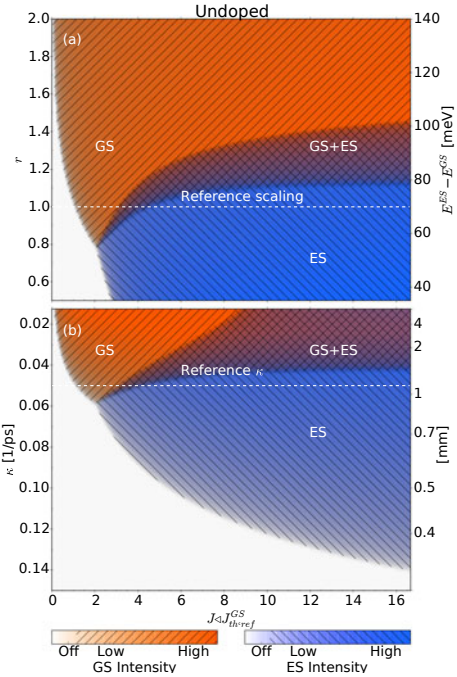

Figure 4.15: Lasing regime for GS (orange) and ES (blue) versus pump currents and confinement scaling factor r (a) and optical losses κ (b) obtained by numerical simulation. The two-state lasing is visible (cross hatched area). The reference lasing intensities for size $r = 1$ and $\kappa = 0.05ps^{-1}$ are seen in Fig. 4.10. GS quenching is only observed for some sizes r, others exhibit only ES lasing (shallow dots), no ES lasing (deep dots) or only a saturation of the GS intensity. Also visible is the decreased lasing threshold for lower losses. Parameters not varied here are given in Tab. 4, with microscopically calculated scattering rates as in App. A.2 with hole capture reduced to 5%. ©(2015) IEEE. Reprinted, with permission, from [ROE14]

Fig. 4.15 (a) shows the lasing regimes for GS and ES for different QD confinement and pump current. The parameters corresponding to the reference light curve of Fig. 4.10 are marked by the white dashed line in the parameter-plots. White areas correspond to no active lasing, while orange areas exhibit GS lasing and blue areas ES lasing. The two lasing modes are also hatched differently, and their overlay is visible as a mixing of colours and the overlap of the hatching schemes.

As seen in Fig. 4.15 (a), for greater energy separation, e.g. higher r, no GS quenching will be observed and ES lasing might not even start. This is due to the high confinement leading to lower ES occupations, as the GS is energetically more favourable. On the other hand, smaller energy spacing suppresses GS lasing and enhances ES filling. As the ES has a higher gain, it will always dominate when occupations of ground and excited state levels are similar. Hence the lower regions of Fig. 4.15 (a) display pure ES lasing.

Figure 4.15 (b) shows the variation of optical losses κ. The white dashed line again denotes the reference of Fig. 4.10 for $\kappa = 0.05\text{ps}^{-1}$. As expected from the analytic results shown in Fig. 4.6, the lasing threshold increases for higher losses, e.g. shorter cavities, while the onset of two-state lasing decreases for higher losses. Above a certain loss value $\kappa \simeq 0.06\text{ps}^{-1}$, only ES lasing can be observed, as the GS gain gets too weak to counter the optical losses. This corresponds to the parts of Fig. 4.6, where the GS lasing regime recedes further for lower gain, until only solitary ES lasing is observed. Contrastingly, for low losses (long cavities), the overlap between ES and GS lasing regime is so large, that the electron-hole ratio never surpasses the critical value necessary for GS quenching. Followingly the upper regions of Fig. 4.15 (b) exhibit stable two-state lasing.

As discussed in Sec. 3.3.1, this is in agreement with the experimental findings of Ref. [MAR03a]. Long cavities have lower losses κ (see second y-axis in Fig. 4.15 (b)). They found a critical length ℓ, below which only ES lasing was present, intermediate lengths with two-state lasing and an increasing threshold current for the ES lasing for larger devices. This has also been independently confirmed in Ref. [CAO09] and Ref. [LEE11c] and the need of short cavities is also mentioned in Ref. [VIK07a]. This is nicely reproduced by the parameter studies of Fig. 4.15. Additionally, Ref. [MAX13] shows the GS and ES threshold currents versus cavity lengths as measured by Maximov et al. and this also exhibits a good agreement with the numerical findings of this work. Higher cavity lengths favour GS lasing and below a certain critical length, only ES lasing is present.

4.3.2. Influence of Doping

Doping has been shown to influence two-state-lasing behaviour [MAX13] and lasing thresholds [TON06]. This will now be investigated further with the numerical model and be compared to the undoped case.

Dopings within this work have been simulated with 10 extra charge carriers per QD. Charge conservation is now maintained with an offset, accounting for the extra electrons or holes added by doping [LUE10, KOR10]. Increased intrinsic losses R^W_{loss} for the QW or photons κ_{int} were not used, even though they could be introduced by the higher defect rate in doped materials. Yet the focus shall be set on the charge carrier dynamics, and not be complicated by changing more than one parameter at a time.

When comparing the lasing regimes of Fig. 4.16 to the undoped Fig. 4.15, n-doping increases the lasing threshold. This is in accordance with previous theoretical results [TON06] and can be explained by the different hole and electron dynamics. As seen in Fig. 4.11, electron states are always fuller than their hole counterpart. So

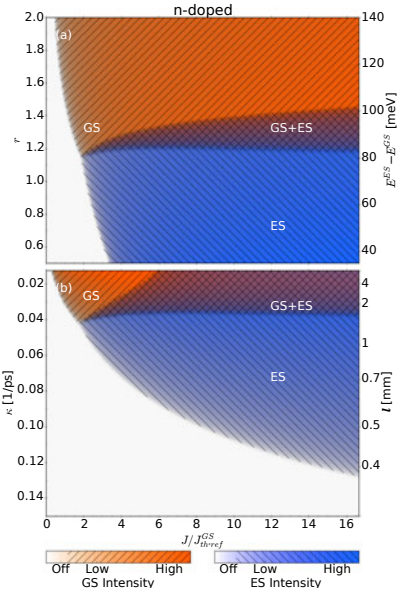

Figure 4.16: Lasing regime for GS (orange) and ES (blue) versus pump currents J and confinement scaling factor r (a) and optical losses κ (b) for n-doped QDs. The two-state lasing is visible (cross hatched). The n-doped QDs show a higher lasing threshold as compared to undoped (Fig. 4.15) and a smaller two-state lasing regime. Solitary ES lasing is more common, as the high electron to hole ratio needed for GS suppression is already intrinsically present. Parameters as given in Tab. 4, with microscopically calculated scattering rates as in App. A.2 with hole capture reduced to 5%. ©(2015) IEEE. Reprinted, with permission, from [ROE14]

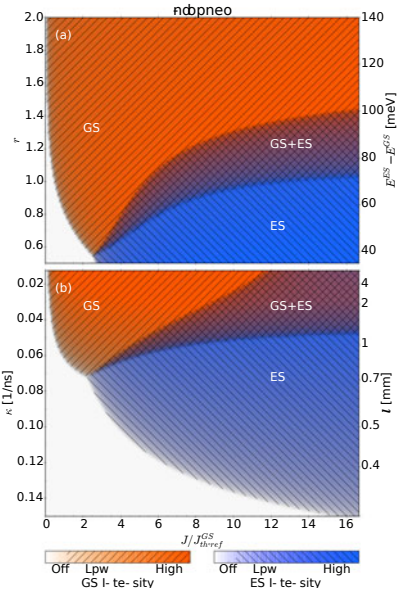

Figure 4.17: Lasing regime for GS (orange) and ES (blue) versus pump currents J and confinement scaling factor r (a) and optical losses κ (b) for p-doped QDs. The two-state lasing is visible (cross hatched). The p-doped QDs exhibit a lower lasing threshold as compared to undoped QDs (Fig. 4.15) and a broader two-state lasing regime. GS lasing is enhanced and the ES lasing threshold is higher. Parameters not varied here are given in Tab. 4, with microscopically calculated scattering rates as in App. A.2 with hole capture reduced to 5%. ©(2015) IEEE. Reprinted, with permission, from [ROE14]

naturally, adding more electrons does not significantly increase occupations in the QD, but mostly in the well w_e. This leads to higher non-radiative loss processes, which always also remove a hole from the system. Therefore, n-doping increases losses without aiding lasing, which leads to an overall increase in the lasing threshold.

Somewhat counterintuitively, GS quenching is observed for a smaller range of parameters. On first thought, one could suspect that the additional electrons introduced by n-doping are aiding the hole-depletion process. So a broader range of GS quenching could be expected. That this is not the case in Fig. 4.16 can be explained by the broader ES lasing regime. In general, doping becomes less important

for high pump currents J, so that n-doped and undoped will converge to similar electron-hole ratios far above lasing threshold. This is reflected by the fact that the high -current right-hand sides of the n-doped Fig. 4.16 and the undoped Fig. 4.15 look the same. On the other hand, n-doping significantly influences the low current dynamics. The n-doped samples already start with more electrons than holes and will then start to lase directly in the ES, with no intermediate two-state lasing. GS quenching is therefore not observed, because the GS already starts suppressed for a broader parameter range.

Oppositely, adding additional holes via p-doping (Fig. 4.17) leads to a smaller lasing threshold. Most holes that are intrinsically present will relax into the QD GS and aid the onset of GS emission. As opposed to electron occupations, hole occupations are far from saturation, so adding additional holes fills the GS faster.

P-doping also leads to higher GS output power and broader GS lasing regime. Opposite to the effects of n-doping, initial GS lasing and subsequent two-state lasing is observed for a greater parameter range. This is once again caused by the doping-carriers dominating the low-current region, where additional holes facilitate GS lasing. Subsequently, the steady state solutions converge to the undoped-cases when injected carriers start to outweigh the doping carriers for high injection currents J. Followingly, GS quenching is observed for a broad parameter range. P-doping therefore enhances GS quenching.

The reduction of the GS lasing threshold by p-doping has also been theoretically predicted by Ref. [JIN08] for some parameter sets. On the contrary, the experiments of Ref. [ALE07] and [MIK05] show an increase of the lasing threshold for p-doping, but this is attributed to the increased optical losses, so that the results of the numerical simulation are confirmed by real world QD behaviour.

4.3.3. Temperature and ES gain dependence

Furthermore, the background temperature T and ES gain g_{ES} are also parametrically studied. Here the degeneracy caused restriction of $g_{ES} = 2g_{GS}$ used so far is lifted and the ES gain is treated as an independent parameter. On a microscopic level this can compensate the effects of different electric dipole moments for the two possible optical transitions and, on the other hand, can also model the scenario of different mirror reflectivities for the GS and ES wavelengths.

The temperature enters the numerical simulations via the detailed balance condition, modifying the Fermi-function and hence the difference of in- and out-scattering. A higher temperature will lead to a broader Fermi-distribution and therefore equalise the GS and ES occupations, while a lower temperature leads to a concentration of carriers in the GS. Also, there is no self-heating included in these simulations. Temperature changes of more than 50 K would also significantly change the scattering behaviour of the in-scattering rates, The ES gain variation directly influences the ES lasing threshold, but has otherwise no direct effect on the system.

Figure 4.18 (a) shows the lasing intensities for GS (orange) and ES (blue) versus pump current and background temperature for undoped QDs. In contrast to the cavity length and QD size plots, the transition from two-state lasing to solitary ES lasing is less pronounced in the temperature plots. Especially in the lower tempera-

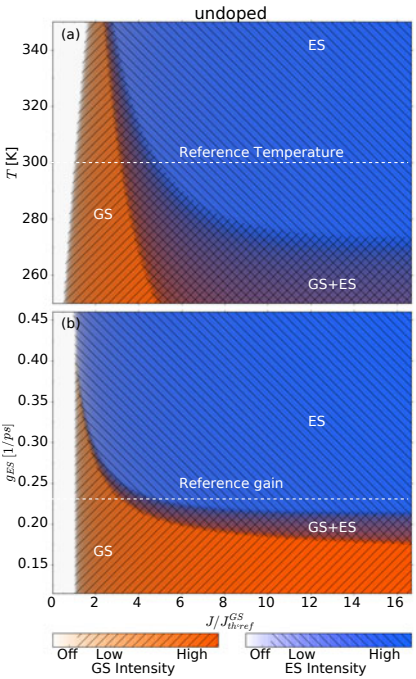

Figure 4.18: Lasing regime for GS (orange) and ES (blue) versus pump currents J and temperature T (upper panel) and ES gain g_{ES}. The ES gain was treated as an independent parameter, so that at $g_{ES} = 0.115ps^{-1}$ (lowest limit of (b)) it is equal to the GS gain g_{GS}. The reference lasing intensities for size $T = 300$K and $g_{ES} = 0.23ps^{-1}$ are seen in Fig. 4.10. GS quenching is only observed for some temperatures and gains, others exhibit only ES lasing (high ES gain), no ES lasing (low ES gain) or only a saturation of the GS intensity (lower temperatures). Also visible is the decreased lasing threshold for lower temperatures. Parameters not varied here are given in Tab. 4, with microscopically calculated scattering rates as in App. A.2 with hole capture reduced to 5%.

ture regions ($\sim 270K$) GS lasing is sustained over a broad current range. Therefore, changing the temperature significantly changes the extent of the two-state lasing regime, with a faster GS quenching at higher temperatures. Low temperature delays the onset of ES lasing as well and lowers GS lasing thresholds.

This is in good agreement with the experimental results of Maximov *et al.*. Fig. 4 of Ref. [MAX13] shows their experimental measurements of the threshold current densities for the GS (circles) and ES (squares). They also measured p-doped QDs and its effect on two-state lasing.

The ES gain dependence of Fig. 4.18 (b) is as expected: Higher g_{ES} enhances the ES lasing intensity and reduces ES threshold currents, while lower g_{ES} delays the onset of two-state lasing. Note, that on the lower border $g_{ES} = g_{GS} = 0.115ps^{-1}$ and that ES lasing is absent. Furthermore, it is visible that the GS lasing threshold is independent of ES gain - as the border between GS lasing regime (red) and no lasing (white) is vertical in (b).

So as done in the previous section, a p-doped and an n-doped QD ensemble is also simulated for different temperatures and ES gains. Fig. 4.19 shows the p-doped parameter plots. GS lasing is once again enhanced by the p-doping of QDs, as the holes are the rare species of carriers. The additional holes in the system delay hole-depletion, so that a wide array of parameters start to lase on the GS and then switch

to the ES. ES lasing thresholds are greatly increased, which is in good qualitative agreement with Fig. 4 of Ref. [MAX13], where the temperature dependence of a p-doped sample was also compared to an undoped QD sample.

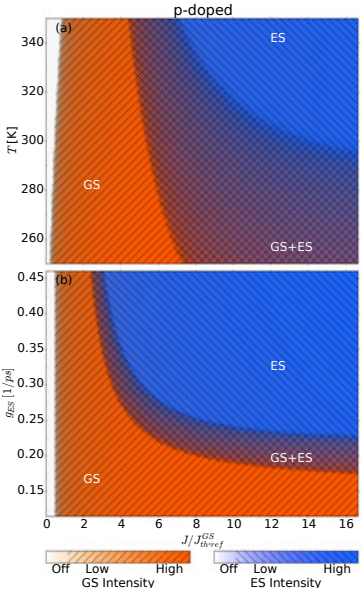

Figure 4.19: Lasing regime for GS (orange) and ES (blue) versus pump currents J and Temperature T (a) and ES gain g_{ES} (b) for p-doped QDs. In comparison to the undoped case (see Fig. 4 of Ref. [MAX13]), ES lasing is weakened and GS quenching happens for a broader set of parameters. Also visible is the overall decreased lasing threshold.

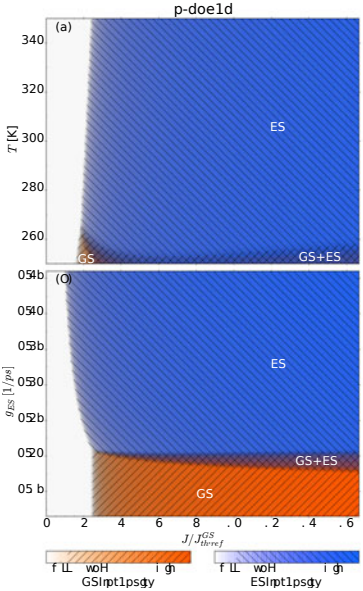

Figure 4.20: Lasing regime for GS (orange) and ES (blue) versus pump currents J and Temperature T (a) and ES gain g_{ES} (b) for n-doped QDs. In comparison to the undoped case (see Fig. 4 of Ref. [MAX13]), ES lasing is enhanced and GS quenching happens for fewer parameters. Also visible is the decreased lasing threshold for higher ES gains, if and only if the ES is the first to lase.

Finally, n-doping increases thresholds and enhances ES lasing as shown in Fig. 4.20. The independence of the GS lasing threshold from the ES gain g_{ES} can also be seen in (b), where the overall lasing thresholds is only increased if and only if the ES is the first to lase. As soon as the ES lasing regime (blue) borders the no-lasing regime (white), the threshold currents starts to decrease with increasing ES gain. There also appears to be a region in temperature space, where a reappearance of the GS can be observed. The initial n-doping must be suppressing the hole fraction to such a low value, that it actually recovers for higher values. This would, in any experiment, probably be completely washed out by the high fraction of defects introduced through doping and not be observable.

To conclude these numerical parameter studies, it has become clear that GS quenching is a transition phenomenon in parameter space. GS quenching is the specially tuned case of parameters that lie inbetween the regions of purely ES lasing and purely GS lasing devices. A stable two-state lasing over a broad current range can be achieved by the right choice of parameters and might be of interest for anybody who wishes to fabricate two-state lasing devices. As opposed to QD size and ES gain, the cavity length and operation temperature can be changed during experimental operation and the numerical results presented in this section are in good agreement with the published experimental data.